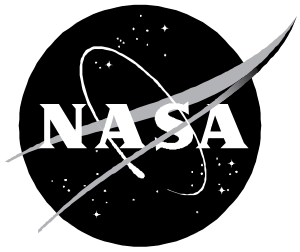

NASA Technical Memorandum 4726

Subsonic Aerodynamic Characteristics of a Circular Body Earth-to-Orbit Vehicle

Roger A. Lepsch, Jr. and George M. Ware
Langley Research Center • Hampton, Virginia

Ian O. MacConochie
Lockheed Engineering & Sciences Company • Hampton, Virginia

National Aeronautics and Space Administration
Langley Research Center • Hampton, Virginia 23681-0001

July 1996

Available electronically at the following URL address: http://techreports.larc.nasa.gov/ltrs/ltrs.html

Printed copies available from the following:

NASA Center for AeroSpace Information
800 Elkridge Landing Road
Linthicum Heights, MD 21090-2934
(301) 621-0390

National Technical Information Service (NTIS)
5285 Port Royal Road
Springfield, VA 22161-2171
(703) 487-4650

Summary

The circular body configuration is a generic shape applicable to single- or multistage reusable Earth-to-orbit transports. The principal attribute of the configuration is its low structural weight for a given propellant loading. The low weight results from the utilization of simple, structurally efficient, circular cross-section tanks as part of the body. A thick, clipped delta wing is the major lifting surface. For directional control, three different vertical fin arrangements were investigated: a conventional aft-mounted center vertical fin, wingtip fins, and a nose-mounted vertical fin. The test was conducted in the 7- by 10-Foot High-Speed Tunnel at the Langley Research Center at Mach number 0.3.

The results of the investigation indicated that the configuration was longitudinally stable about the estimated center-of-gravity position of 72 percent of body length. The model had sufficient pitch-control authority with elevators to produce stable trim for a wide range of angle of attack. The maximum trimmed lift-drag (L/D) ratio for the aft center-fin configuration was less than 5, whereas the other configurations had values above 6.

The aft center-fin configuration was directionally stable for all angles of attack tested. The wingtip and nose fins were not intended to produce directional stability, and did not. The rudder-like surfaces (controllers) on the wingtip fins and the all-moveable nose fin were designed as active controls to produce artificial directional stability. These controls were effective in producing yawing moment. Small rolling-moment values resulted from yaw control of the nose fin. Large adverse rolling-moment increments resulted from wingtip-fin controller deflection above an angle of attack of 13°. Flow visualization indicated that this was most likely caused by the influence of wingtip-fin controller deflection on wing flow separation.

Introduction

The National Aeronautics and Space Administration (NASA) is investigating concepts for future space transportation systems. The studies have included single- and multistage-to-orbit designs (refs. 1–5). Structural weight is a critical factor in the performance and cost of these designs. To minimize weight, circular cross-section propellant tanks were integrated into a vehicle concept as load-carrying structure. The intent was to produce a simple configuration with a low weight-to-volume ratio. Referred to as the circular body vehicle (CBV), this design is a generic configuration that is an example of a single-stage vehicle or an orbiter or booster element of a multistage system. The vehicle has an aft-mounted clipped delta wing and an estimated center of gravity at 72 percent of the body length. (The aft location results from the heavy rocket engines at the base and empty propellant tanks in the forward body.) This center-of-gravity location limits the moment arm of a conventional vertical tail, resulting in the need for a relatively large tail size when both stability and control are desired.

Alternate yaw-control devices were tested in an effort to further reduce weight. The devices were wingtip fins and an all-moving nose-mounted fin. The wingtip fins house rudder-like surfaces (wingtip-fin controllers) that are designed to be continually deflected for stability augmentation. These fins can be small because they are not required to provide natural directional stability, thereby saving weight. (See ref. 6 for a description of wingtip-fin controllers and their use.) The all-moving nose-mounted fin is designed to act in a manner similar to the wingtip fins. Sensors detect deviation from the desired flight path and signal the nose fin to deflect to drive the CBV back on course or prevent the vehicle from diverging. A small fin is possible because of the large moment arm available. The structural characteristics and hypersonic heating characteristics of the CBV are shown in references 7 and 8, respectively. Summary subsonic characteristics appear in reference 9, and supersonic characteristics appear in reference 10.

The present investigation was made to determine in more detail the subsonic aerodynamic characteristics of the CBV during unpowered entry from Earth orbit. Three yaw control devices were tested: a conventional aft-mounted center vertical fin, wingtip fins, and a nose-mounted fin. The large aft center fin is the only fin configuration designed to give the CBV directional stability (positive C_{n_β}). Separate pitch- and roll-control surfaces were mounted on the wing trailing edge, and a body flap extended aft of the fuselage. The test was conducted in the Langley 7- by 10-Foot High-Speed Tunnel at Mach number 0.3 and a Reynolds number of 8.7×10^6, based on body length.

Symbols

The axis system used in the investigation is presented in figure 1. The data are normalized by the wing planform area (including the body flap), the wingspan, and the length of the wing mean aerodynamic chord. The moment reference center was located at the proposed vehicle center of gravity, which is at 72 percent of body length from the nose.

b	wing span, in.
C_D	drag coefficient, Drag/qS_{ref}
C_L	lift coefficient, Lift/qS_{ref}
C_l	rolling-moment coefficient, Rolling moment/$qS_{\text{ref}}\,b$

C_m	pitching-moment coefficient, Pitching moment$/qS_{\text{ref}}\bar{c}$
C_n	yawing-moment coefficient, Yawing moment$/qS_{\text{ref}}\,b$
C_Y	side-force coefficient, Side force$/qS_{\text{ref}}$
$\bar{c}$	wing mean aerodynamic chord, in.
L/D	lift-drag ratio
l	body length, in.
M	Mach number
q	free-stream dynamic pressure, lb/in^2
S_{ref}	wing planform area (projected to body centerline including body flap), in^2
X	longitudinal body axis
Y	lateral body axis
Z	vertical body axis
α	angle of attack, deg
β	angle of sideslip, deg
ΔC_l	change in rolling-moment coefficient
ΔC_n	change in yawing-moment coefficient
ΔC_Y	change in side-force coefficient
δ_a	aileron-control deflection angle $(\delta_{a,L} - \delta_{a,R})/2$, deg
$\delta_{a,L}$	left wing aileron deflection angle (positive when deflected downward), deg
$\delta_{a,R}$	right wing aileron deflection angle (positive when deflected downward), deg
δ_e	elevator deflection angle (positive when deflected downward), deg
δ_n	nose-fin deflection angle (positive when deflected with trailing edge to right), deg
δ_r	rudder deflection angle (positive when deflected with trailing edge to left), deg
δ_{SB}	speed-brake deflection angle, deg
δ_{TF}	wingtip-fin controller deflection angle positive when deflected with trailing edge to left), deg

Stability derivatives:

C_{l_β}	$\Delta C_l/\Delta\beta$ taken at $\beta = 0°$ and 4°, per deg
C_{n_β}	$\Delta C_n/\Delta\beta$ taken at $\beta = 0°$ and 4°, per deg
C_{Y_β}	$\Delta C_Y/\Delta\beta$ taken at $\beta = 0°$ and 4°, per deg

Subscripts:

max	maximum value
ref	reference

Description of Model

A photograph of the circular body model in the Langley 7- by 10-Foot High-Speed Tunnel is presented in figure 2(a), and a sketch of the CBV with the three fin arrangements tested is shown in figure 2(b). Dimensional information is given in figure 3 and table 1. The model consisted of a spherically blunted ogive nose blended into a large circular cross-section body with a clipped delta wing with a 47° of sweep mounted on the far aft underside. A body flap extended aft from the lower body. The wing, which had a National Advisory Committee for Aeronautics (NACA) 0010-64 airfoil, was equipped with elevator surfaces on the inboard portion of the unswept trailing edge and small aileron surfaces on the outboard portion. Three vertical fin configurations were investigated: (1) a large conventional center fin on the upper aft fuselage, (2) a small vertical fin near the fuselage nose, and (3) a small fin on each wingtip. The aft center fin had a wedge airfoil shape with a rounded leading edge and a blunt trailing edge, as did each wingtip fin. The nose fin had a modified NACA 0015 airfoil with a rounded trailing edge truncated at 45 percent of the airfoil chord.

The elevators could be deflected from 14° to −20°. The ailerons were tested at ±5°. The body flap was not deflected in these tests. The deflected yaw-control surfaces on the center vertical fin were simulated by wedges of 7.5° and 15° attached to the fin. This configuration represents a split control surface with one half deflected, while the other half remains undeflected. The wingtip-fin control surfaces, referred to as controllers, are flush-mounted panels designed to be deflected in an outward direction only. Controller deflections were simulated by angled plates of 20°, 40°, and 60°. The controllers act as yaw generators when a single surface is deflected outward. Deflection of the nose fin for yaw-control evaluation was accomplished by pivoting it about its 0.25-chord station. In addition to pitch-, roll-, and yaw-control surfaces, various speed brake controls were investigated. (See fig. 2(b).) With the aft center fin, the brake system consisted of a flared split rudder with equal deflection on each side of the fin. With wingtip fins, the brakes were simultaneous outward deflections of both wingtip-fin controllers. For the nose-fin configuration, aft side-body-mounted panels were deflected.

Apparatus, Tests, and Corrections

Tests were conducted in the Langley 7- by 10-Foot High-Speed Wind Tunnel, a closed-circuit subsonic atmospheric tunnel with a nominal 7-foot-high by 10-foot-wide test section. A description of the facility appears in reference 11. The test was conducted at a Mach number of 0.3 and a Reynolds number of 8.7×10^6, based on body length. The model was sting

mounted through its base, and forces and moments were measured with an internally mounted strain-gage balance. Model angles of attack and sideslip were corrected for sting and balance deflection under load by wind-off calibration of the system with weights. Tunnel interference corrections caused by changes in jet boundary, buoyancy, flow angularity, and blockage by the presence of the model were applied to the data. To fix the boundary layer laminar-to-turbulent-flow transition point, transition grit was applied on the model according to methods described in reference 12. Number 100 carborundum grit was thinly sprinkled in 1/16-in. bands 1 in. aft of the nose. Number 80 grit of the same width was applied 1 in. downstream of the wing and fin leading edges. The model test pitch range was nominally from −2° to 16°. The model was tested at angles of sideslip of 0° and ±4° over the angle-of-attack range. Data were taken as the model was moved from negative to positive angles. Drag values are presented as measured with no base corrections applied.

To aid in the analysis of the force and moment data, the flow over the model was defined by an oil-flow technique. SAE 40 oil containing a pigment that fluoresces when exposed to ultraviolet light was brushed over the model. The model was positioned in the tunnel at the desired angle of attack. The tunnel was brought up to speed, and after the oil had sufficient time to flow, the tunnel was shut down. The model was illuminated with an ultraviolet light and photographs were taken. The photographs were then used to visualize flow characteristics.

Results and Discussion

Longitudinal Characteristics

Baseline characteristics. Lift, drag, and pitching-moment coefficients and *L/D* are plotted against angle of attack in figure 4 for the model with fins off and with each of the vertical fin arrangements. The lift and pitch data for all configurations are linear up to about $\alpha = 12°$. Above $\alpha = 12°$, a decrease in the lift curve slope indicates the onset of flow separation. The highest lift values for a given angle of attack were obtained with the wingtip-fin configuration. The wingtip fins acted as end plates to increase wing effectiveness. (See ref. 13.) The added wing lift also is seen as a slight increase in longitudinal stability over that of the other configurations. The model with each vertical fin combination or with fins off was longitudinally stable about the 72 percent of body length reference. The very large aft center fin (68 percent of the exposed area of a single wing panel) produced more drag than the other fin arrangements. As a result, the model with the center fin had lower *L/D* values and a positive pitching-moment increment caused by the drag of the fin acting above the model center of gravity. The maximum untrimmed *L/D* ratio for the aft center-fin configuration was about 5, whereas the other configurations had values of about 7.

Oil-flow photographs of the upper surface of the right wing without and with wingtip fins are presented in figures 5 and 6, respectively. The photographs show the onset of flow separation at angles of attack from 10° to 13°. Separation results from outflow toward the wingtip reversing the flow on the wing upper surface near the tip (fig. 5(c)). Separation for the model with wingtip fins on appears to be very similar to the fins-off case.

Pitch control characteristics. Data for elevator deflections of 0°, −14°, and −20° are presented in figure 7. For each fin arrangement, the negatively deflected surfaces produce moments that trim the model to higher angles of attack. Stable trim is possible for all fin arrangements up to about 12° or 14° angle of attack. For the remainder of the test angle-of-attack range, the CBV is neutrally stable or unstable, with the exception of the wingtip-fin configuration, which may have a stable secondary trim point at a higher angle of attack. The control power of the elevators is sufficient to allow stable trim over a wide angle-of-attack range regardless of fin configuration. As pointed out in the previous section, use of the center fin results in a positive increment in pitching moment relative to the other two configurations. The trim angle for the center-fin configuration with neutral elevators is about $\alpha = 2°$, whereas the other configurations trim at $\alpha = 0°$ or −1°. The estimated trimmed $(L/D)_{max}$ is less than 5 for the center-fin model and somewhat greater than 6 for the model with the other two fin arrangements.

By comparing the flow pattern over the wing with (fig. 8) and without (fig. 5) negative elevator deflection, one sees that the upward deflected elevator delays the onset of flow separation. (Compare figs. 5(c) and 8(c).) A decrease in flow circulation is consistent with the pressure rise on the wing upper surface that would result from an upward elevator deflection.

Speed-brake effects. Three different speed-brake systems were tested on the CBV model, and data from those tests appear in figure 9. Speed brakes are used by a gliding unpowered spacecraft as an energy management device to adjust cross range and target the landing site. For the model with the aft center-fin arrangement, the split rudder acted as a speed brake. Data are presented with the brake open 7.5° and 15° on either side from the closed position (fig. 9(a)). The brake effectively increased drag, but lift decreased somewhat because of downforce generated by the fin. The downforce is the vertical component of the pressure force acting on the

flared split-rudder surfaces, which have a significant projected area in the horizontal plane. The increase in drag above the model center of gravity again produced a large nose-up pitching moment. As a result, the trim angle of attack shifted from about 2° with speed brakes undeflected to 9° with speed brakes set at 15°. If speed brakes are used on the CBV in this fashion, a compensating elevator deflection will have to accompany brake deflection.

The effect of wingtip-fin-mounted speed brakes is presented in figure 9(b). Because the surfaces were relatively small, deflections up to 60° were tested. The brakes extended out from the wingtips and were effective in producing drag increments linear with speed-brake deflection. The line of action of the drag increment from the brakes was close to the estimated center of gravity, so little change in pitching moment resulted. Their use also delayed the onset of flow separation, as can be seen by examining the lift and moment curves in the 12° to 17° angle-of-attack range.

The speed brakes for the nose-fin model were mounted on the sides of the body over the wing. Figure 9(c) shows that deflecting the side-body brakes produced drag increments linear with deflection. However, the brakes were largely ineffective in the upper portion of the angle-of-attack range. Also, lift was reduced as the brakes were deflected. Deflection of the brakes in such close proximity to the wing upper surface disturbed the flow over the wing, resulting in a small loss of lift. This loss of lift caused the pitching-moment curves to shift slightly upward with speed-brake deflection. These effects are quite different from those found in tests at M = 2.0 to 4.6 (ref. 9). In the supersonic speed range, deflection of the side-body brakes increased drag only slightly and introduced a more significant nose-up pitching moment.

Lateral Characteristics

Lateral-directional stability. The lateral-directional characteristics of the CBV appear in figure 10 in the form of the stability parameters C_{Y_β}, C_{n_β}, and C_{l_β} plotted against angle of attack. Data are shown for the model with all fin configurations and with fins off for an elevator setting of −14°. This elevator setting trims the model at an angle of attack that approximates a landing approach condition.

The CBV with aft center fin was directionally stable, with the value of C_{n_β} increasing slightly over the test angle-of-attack range. The model with the other fin arrangements was, as expected, directionally unstable. The nose fin was directionally destabilizing, whereas wingtip fins generally added C_{n_β} increments. Little difference occurred in the effective dihedral parameter $-C_{l_\beta}$ between the fins off and nose-fin configurations. The center-fin model had negative values of C_{l_β} over the test angle-of-attack range.

Yaw-control effects. Rudder effectiveness for each of the vertical-fin arrangements is presented in figure 11. Yaw control for the aft center-fin configuration (fig. 11(a)) was accomplished by deflecting one half of the split rudder outboard and leaving the other half undeflected. The rudder produced almost constant values of yawing moment across the test angle-of-attack range. The retention of effectiveness at high angles of attack probably was caused by the large size of the center fin, which placed it above the influence of the fuselage and wing. As expected, the size and placement of the fin above the vehicle center of gravity also caused large adverse rolling moments with rudder deflection. The value of the rolling moment, which was about one-third that of the yawing moment at the trim angle of attack of 14°, increased significantly with decreased angle of attack.

The effect of deflecting a wingtip-fin controller is shown in figure 11(b). The data indicate that the yawing moments produced by the controller decreased only slightly with increasing angle of attack up to about 13°. At higher angles, a large increase in adverse rolling-moment increment occurred. A clue to the adverse rolling moment is seen in figure 12 when one compares the flow pattern over the wing with the wingtip-fin controller deflected with the flow pattern with the controller undeflected. The deflected controller reduced the outflow on the wing thereby delaying flow separation near the wingtip. With one controller deflected, an adverse rolling moment resulted from the asymmetric flow conditions over the wings.

The nose fin, placed far forward to take advantage of the long moment arm created by the 72 percent of body length center-of-gravity location, was very effective in generating yawing moment (fig. 11(c)). The effectiveness of the deflected nose fin increased almost linearly with increasing angle of attack. This increased effectiveness is probably due to the increase in cross flow around the circular body as the pitch angle increased. These yawing moments were accompanied by only small rolling moments up to the wing flow-separation angle.

Roll-control effects. Roll control results from differentially deflecting the dedicated aileron-control surfaces on the outer wing trailing edge. The effectiveness values are presented in figure 13 for surfaces set at 5° on the left and −5° on the right. Tests were made with wingtip fins on and off. The wingtip-fin controllers were undeflected.

The data indicate that aileron roll effectiveness increased linearly with angle of attack up to angles where flow separation occurred on the wingtip. Small adverse yawing moments accompanied roll control. The control authority of the ailerons appears to be sufficient to counter the adverse rolling moments noted for the center-fin and wingtip-fin arrangements near the trim angles of attack desired for landing. Insufficient data exist to indicate whether the ailerons would have sufficient control effectiveness to counter adverse roll caused by the center fin at reduced angles of attack.

Concluding Remarks

Tests of a circular body spacecraft model have been conducted in the Langley 7- by 10-Foot High-Speed Wind Tunnel. The design is an option considered for single- or multistage-to-orbit vehicles. The model had a body with a circular cross section and a clipped delta wing. Three vertical fin arrangements were investigated: a conventional aft-mounted center vertical fin, wingtip fins, and a nose-mounted vertical fin.

Results of the investigation indicated that the configuration was longitudinally stable about the estimated center-of-gravity position of 72 percent of body length. The model had sufficient pitch-control authority with elevators to produce stable trim over a wide range of angle of attack regardless of fin arrangement. The maximum trimmed lift-drag ratio for the aft center-fin configuration was less than 5, whereas the other configurations had values above 6.

The aft center-fin configuration was directionally stable for all angles of attack. The wingtip and nose fins were not intended to produce directional stability, and did not. The rudder-like surfaces on the wingtip fins and the nose fin were designed as active controls to produce artificial directional stability. These controls were effective in producing yawing moment throughout the test angle-of-attack range. As expected, deflection of the rudder on the aft center fin produced large adverse rolling moments. Small rolling-moment values resulted from yaw control of the nose fin, whereas large, adverse rolling-moment increments resulted from wingtip-fin controller deflection above an angle of attack of 13°.

Differential deflections of the aileron surfaces on the outboard wing trailing edge were effective in producing rolling moments with wingtip fins on or off. Aileron effectiveness was sufficient to counter the adverse rolling moments noted for the aft center fin and wingtip fin configurations in the angle-of-attack range desired for landing.

NASA Langley Research Center
Hampton, VA 23681-0001
April 18, 1996

References

1. Freeman, D. C., Jr.: The New Space Transportation Begins Today. *Astronaut. & Aeronaut.*, vol. 21, June 1983, pp. 37, 48.
2. Martin, James A.: Orbit on Demand: In this Century If Pushed. *Aerosp. America*, vol. 23, no. 2, Feb. 1985, pp. 46–48.
3. Talay, T. A.: *Shuttle II*. SAE Tech. Paper Ser. 871335, June 1987.
4. Holloway, Paul F.; and Talay, Theodore A.: *Space Transportation Systems—Beyond 2000.* IAF Paper 87-188, Oct. 1987.
5. Talay, Theodore A.; and Morris, W. Douglas: Advanced Manned Launch Systems. Paper presented at *AAAF, DGLR, Royal Aeronautical Society, and ESA Second European Aerospace Conference on Progress in Space Transportation* (Bonn, Federal Republic of Germany), May 22–24, 1989.
6. Powell, Richard W.; and Freeman, Delma C., Jr.: Application of a Tip-Fin Controller to the Shuttle Orbiter for Improved Yaw Control. AIAA-81-0074, Jan. 1981.
7. MacConochie, I. O.; and Klich, P. J.: *Technologies Involved in Configuring an Advanced Earth-to-Orbit Transport for Low Structural Mass*. SAWE Paper 1380, May 1980.
8. Wells, William L.; MacConochie, Ian O.; Helms, Vernon T.; and Raney, David: Heating Rate Distributions at Mach 10 on a Circular Body Earth-to-Orbit Transport Vehicle. AIAA-85-0974, June 1985.
9. Lepsch, R. A., Jr.; and MacConochie, I. O.: Subsonic Aerodynamic Characteristics of a Circular Body Earth-to-Orbit Transport. AIAA-86-1801, June 1986.
10. Ware, George M.; Engelund, Walter C.; and MacConochie, Ian O.: *Supersonic Aerodynamic Characteristics of a Circular Body Earth-to-Orbit Vehicle*. NASA TM-4533, 1994.
11. Peñaranda, Frank E.; and Freda, M. Shannon, eds.: *Aeronautical Facilities Catalogue. Volume 1—Wind Tunnels.* NASA RP-1132, 1985.
12. Braslow, Albert L.; Hicks, Raymond, M.; and Harris, Roy V., Jr.: Use of Grit-Type Boundary-Layer-Transition Trips. *Conference on Aircraft Aerodynamics*, NASA SP-124, 1966, pp. 19–36.
13. Montoya, Lawrence C.; Jacobs, Peter F.; and Flechner, Stuart G.: *Effect of Winglets on a First-Generation Jet Transport Wing. III—Pressure and Spanwise Load Distributions for a Semispan Model at Mach 0.30.* NASA TN D-8478, 1977.

Table 1. Geometric Characteristics of Circular Body Model

Body:	
Length, in.	52.00
Base area, in^2	66.96
Wing:	
Airfoil	NACA 0010-64
Mean aerodynamic chord (reference length), in.	16.00
Span (reference span), in.	35.04
Area to body centerline, reference area, in^2	486.60
Area, exposed outside of body, in^2	305.08
Center vertical fin:	
Airfoil	Double wedge
Area, in^2	100.00
Tip fins (each):	
Airfoil	Modified wedge
Area, in^2	11.60
Nose fin:	
Airfoil	Modified NACA 0015
Area, in^2	7.36
Control surfaces (each):	
Elevator area, in^2	25.56
Body flap area, in^2	24.96
Aileron area, in^2	5.84
Wingtip-fin controller and speed brake area, in^2	5.08
Aft center-fin rudder and speed brake area, in^2	25.80
Body speed brake area, in^2	9.72

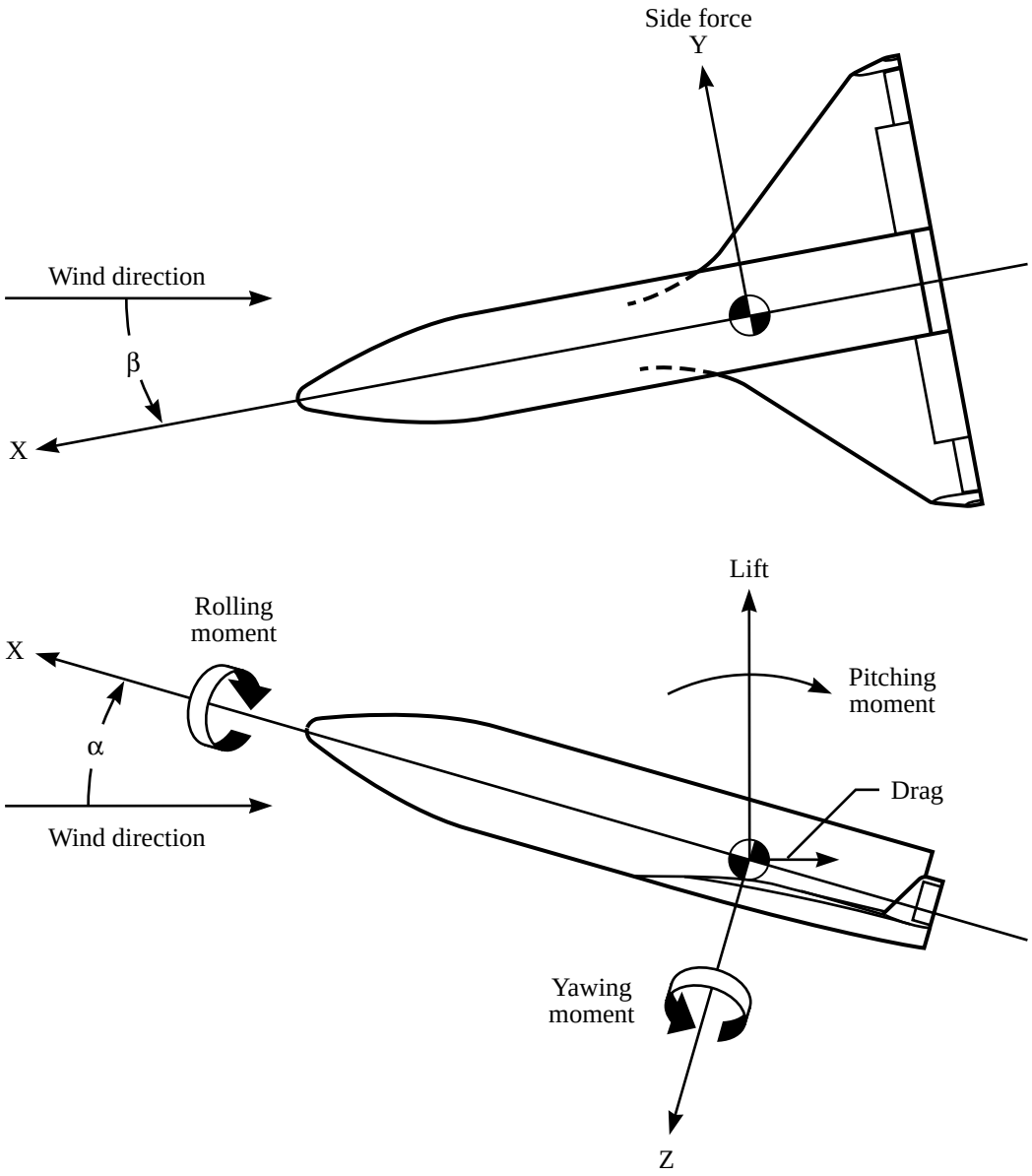

Figure 1. Axis system used in investigation with positive directions of forces and moments.

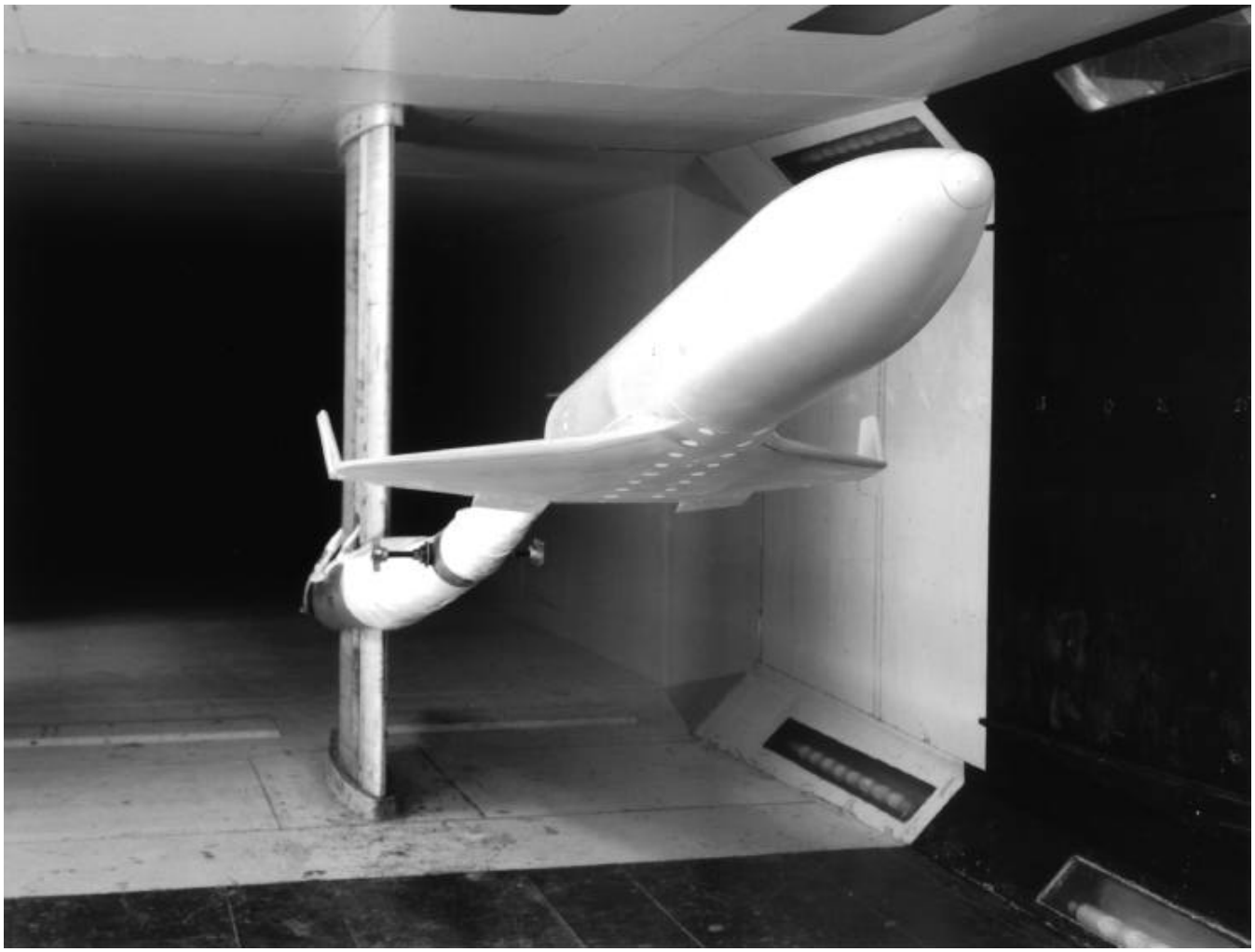

L-84-10,263

(a) Model in Langley 7- by 10-Foot High-Speed Tunnel.

Figure 2. Circular body earth-to-orbit vehicle model.

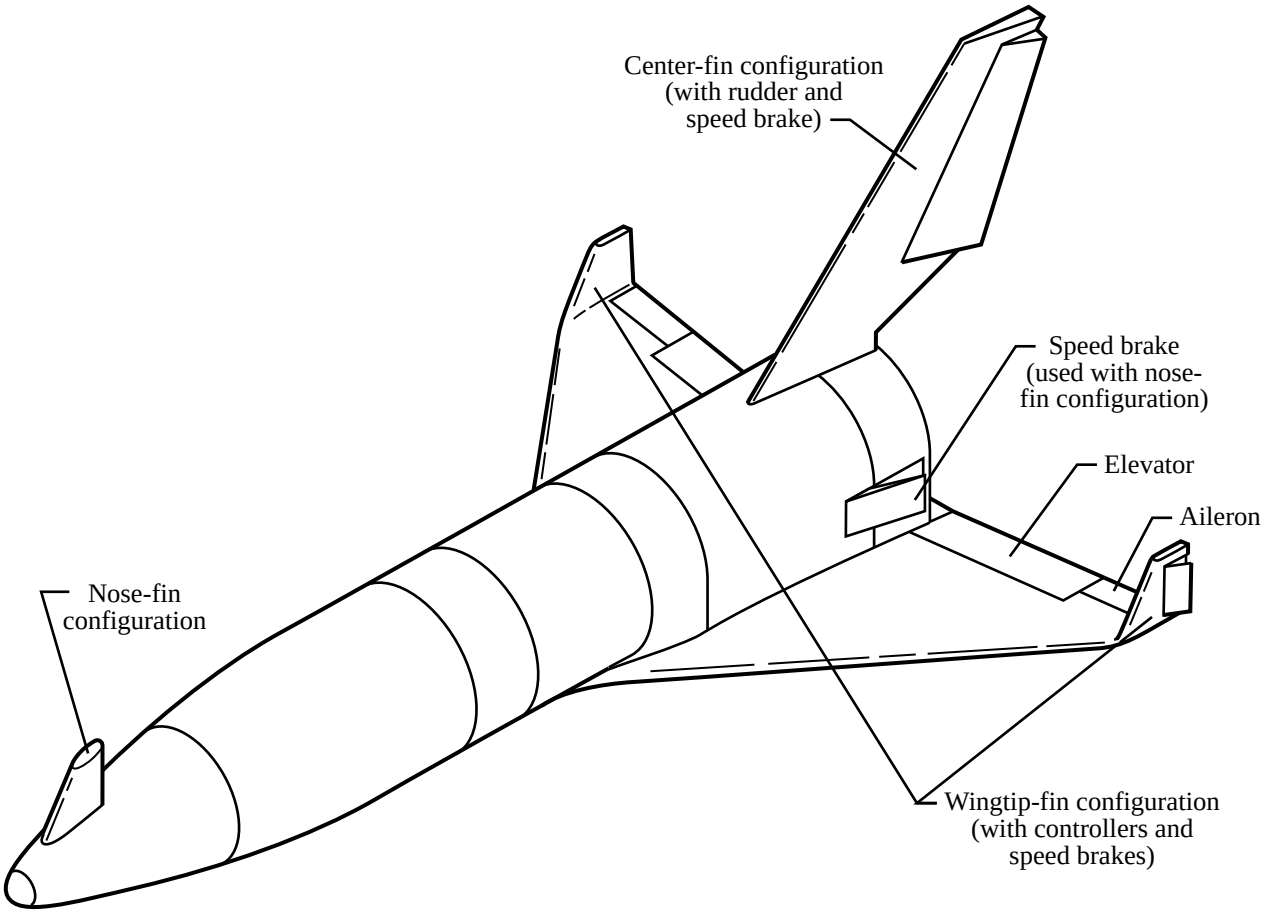

(b) Model showing three fin arrangements investigated.

Figure 2. Concluded.

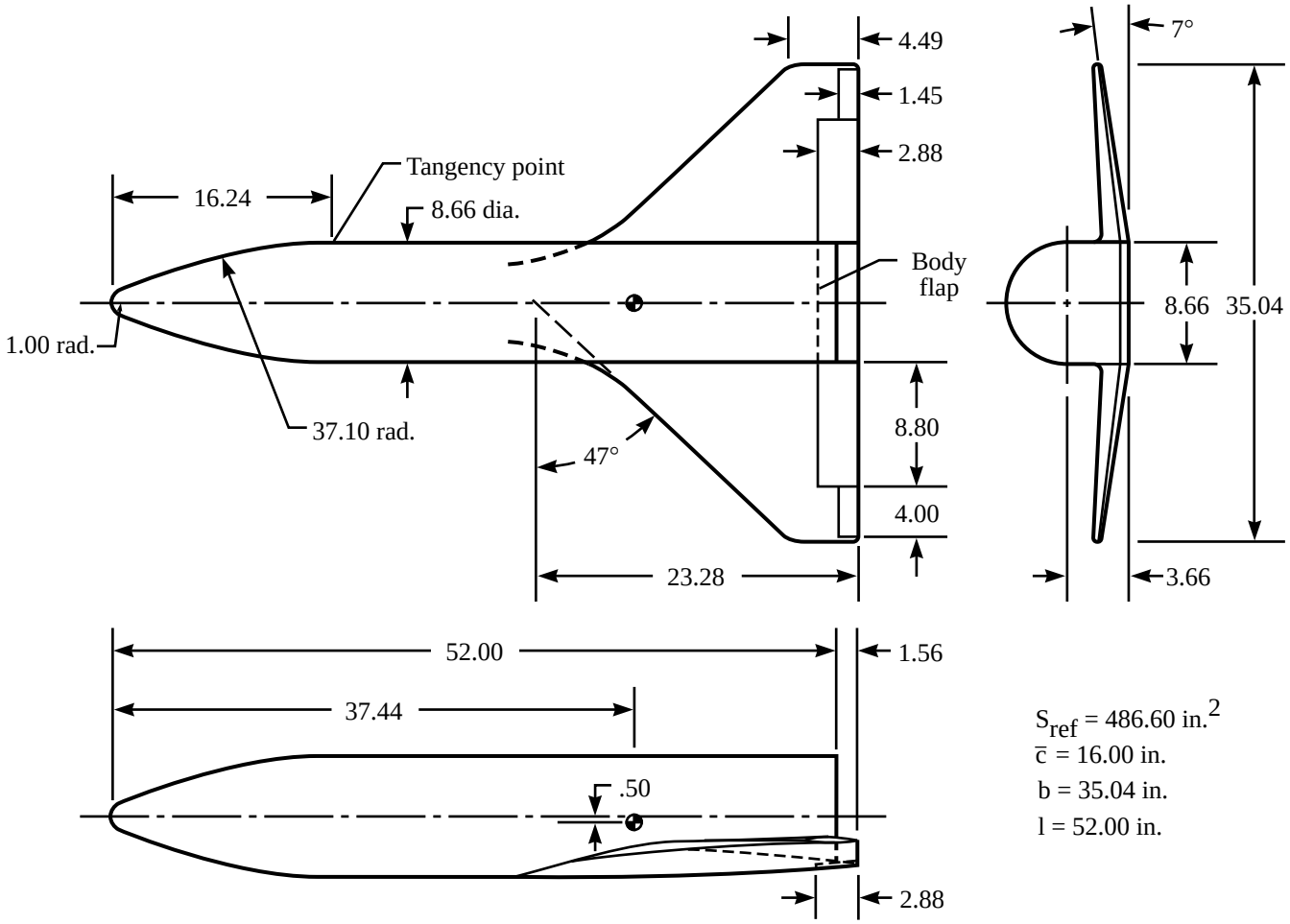

(a) Wing body.

Figure 3. Model used in investigation. All linear dimensions are in inches.

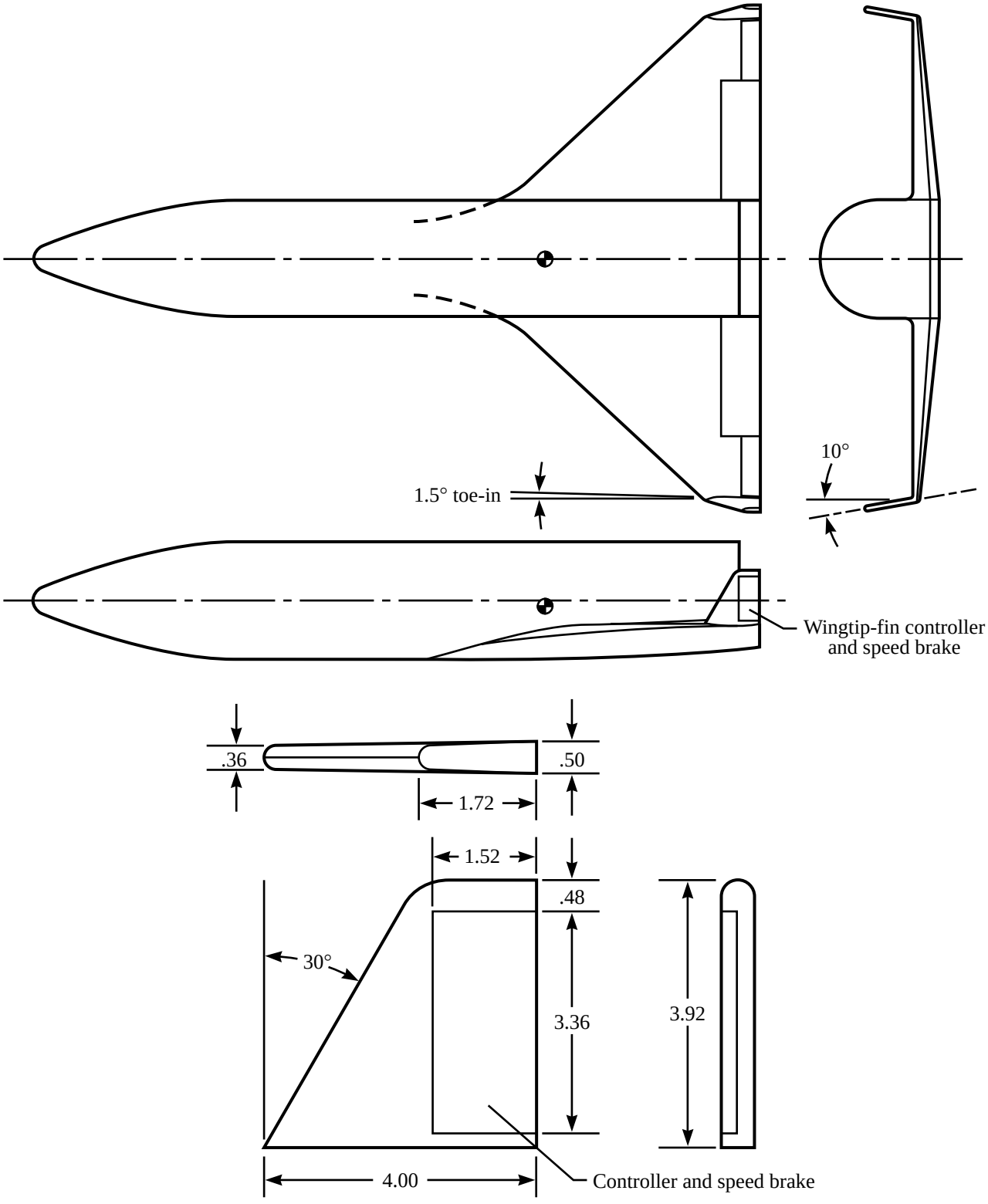

(b) Wingtip fin.

Figure 3. Continued.

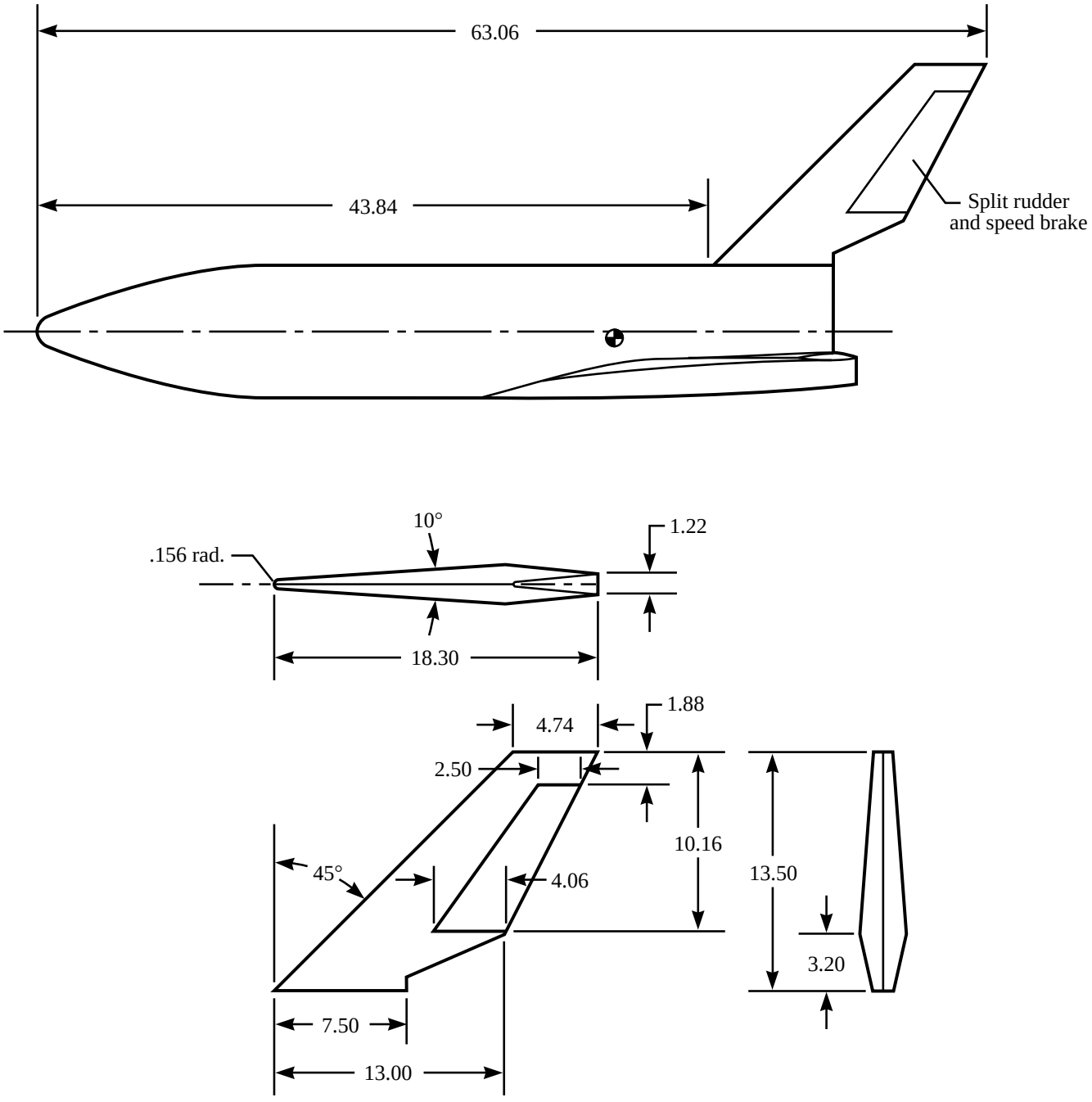

(c) Aft center fin.

Figure 3. Continued.

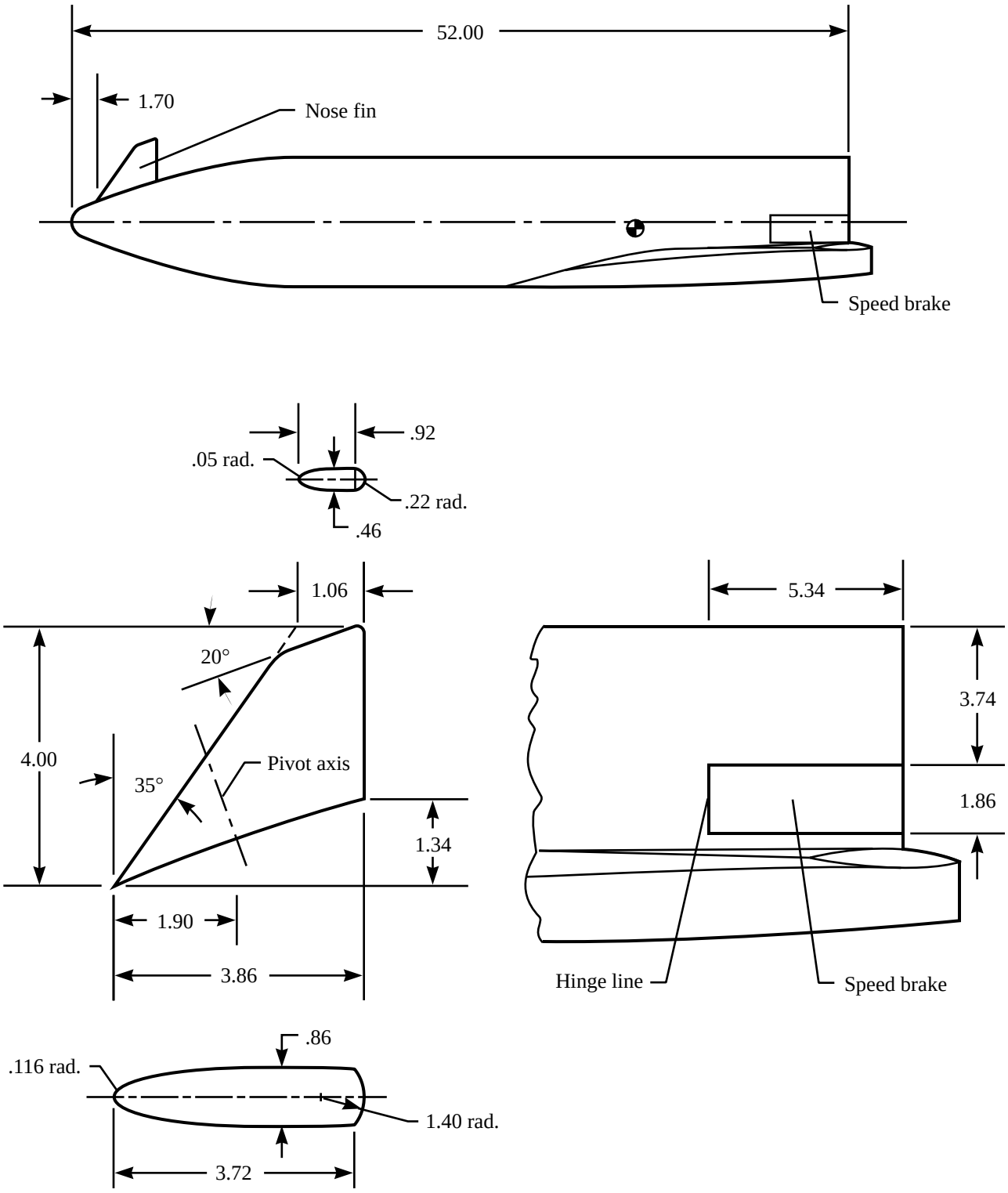

(d) Nose fin.

Figure 3. Concluded.

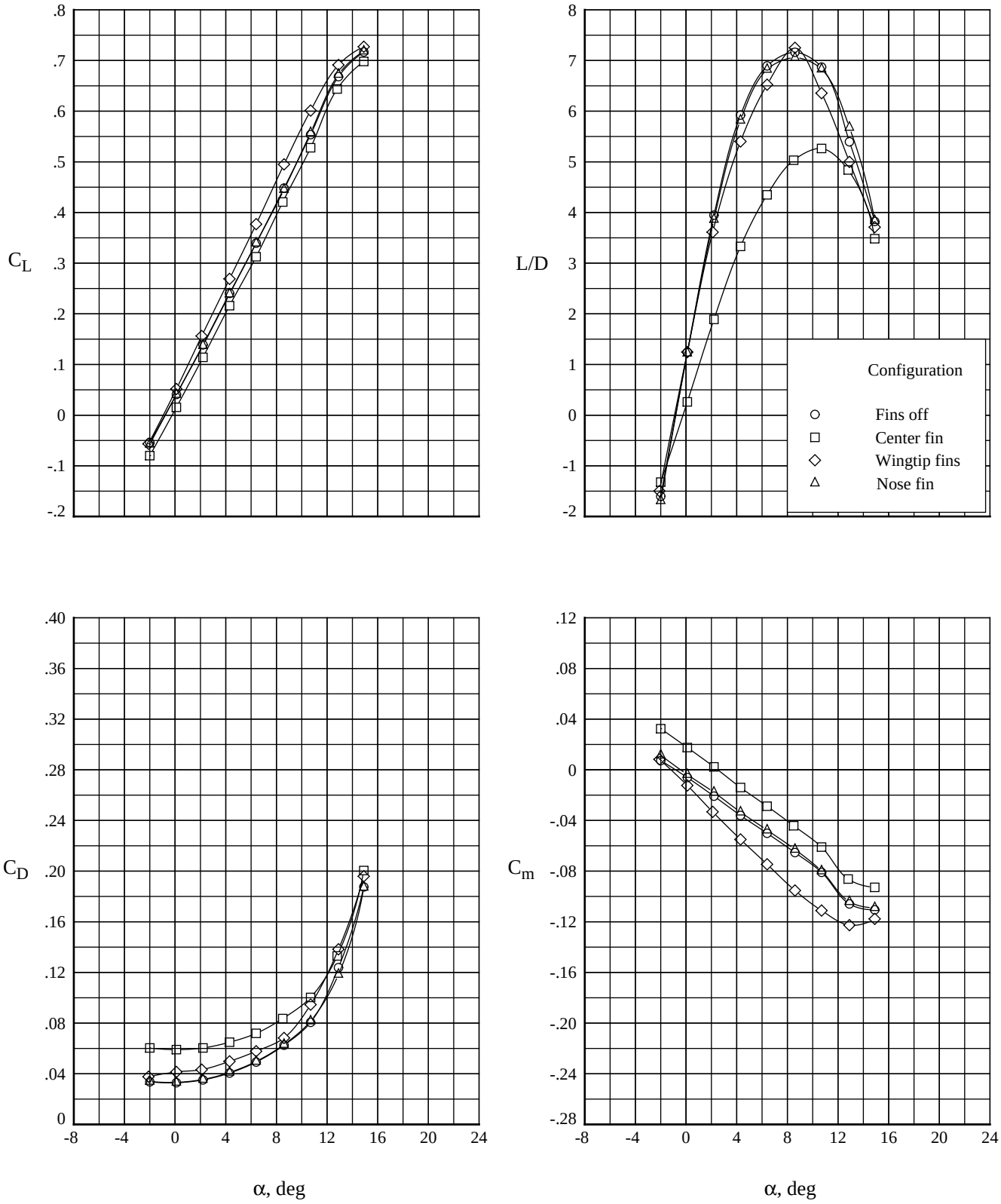

Figure 4. Longitudinal characteristics of circular body model with various fin arrangements. $\delta_e = 0°$.

(a) $\alpha = 6.35°$.

(b) $\alpha = 10.64°$.

(c) $\alpha = 12.80°$.

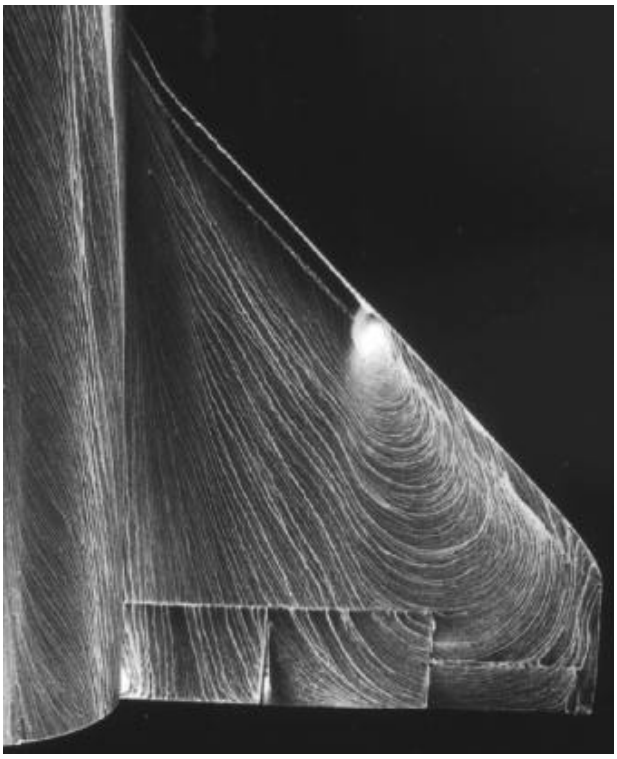

(d) $\alpha = 14.83°$.

Figure 5. Oil flow on fins-off configuration at $M = 0.3$, showing upper surface of right-side wing with $\delta_e = 0°$.

(a) $\alpha = 6.36°$.

(b) $\alpha = 10.72°$.

(c) $\alpha = 12.86°$.

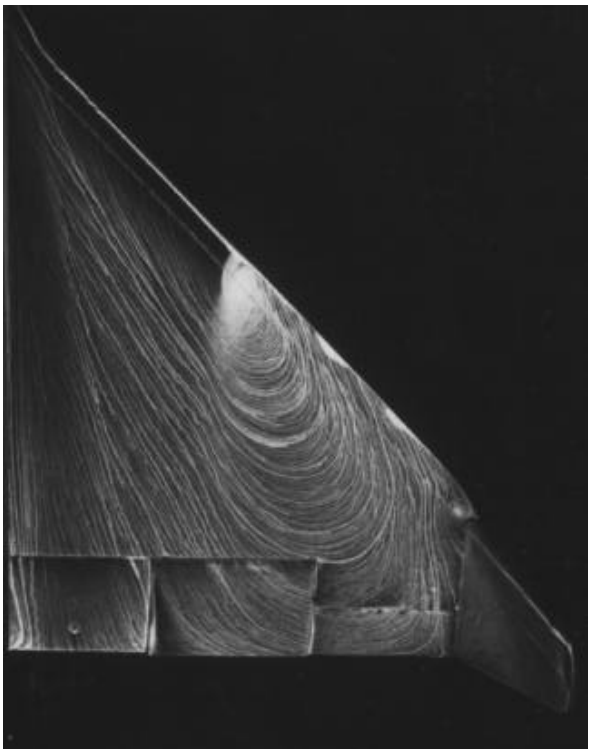

(d) $\alpha = 14.90°$.

Figure 6. Oil flow on tip-fin configuration at $M = 0.3$, showing right-wing upper surface of right-side wing with $\delta_e = 0°$.

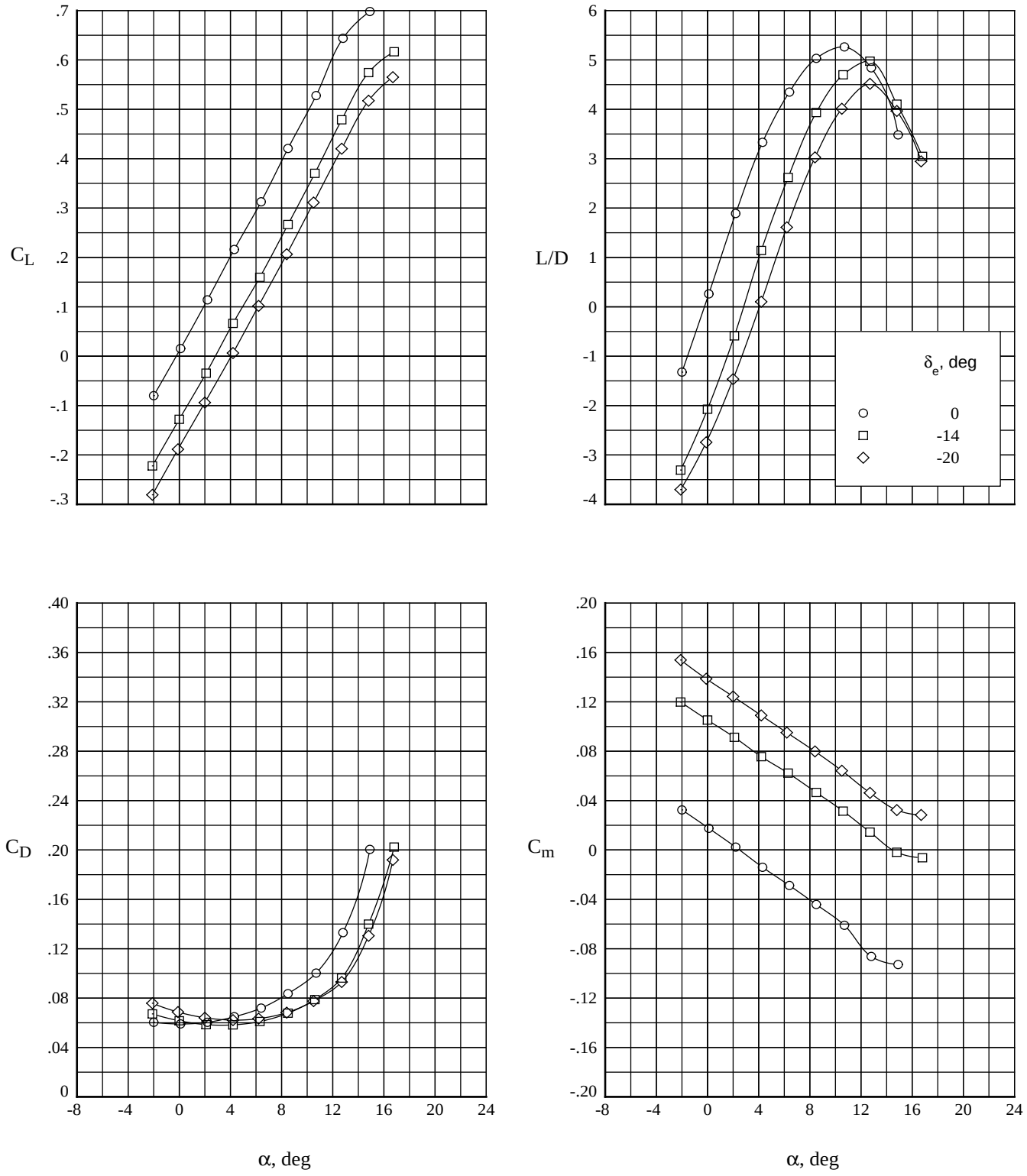

(a) Center fin.

Figure 7. Effect of elevator deflection on longitudinal characteristics of circular body models.

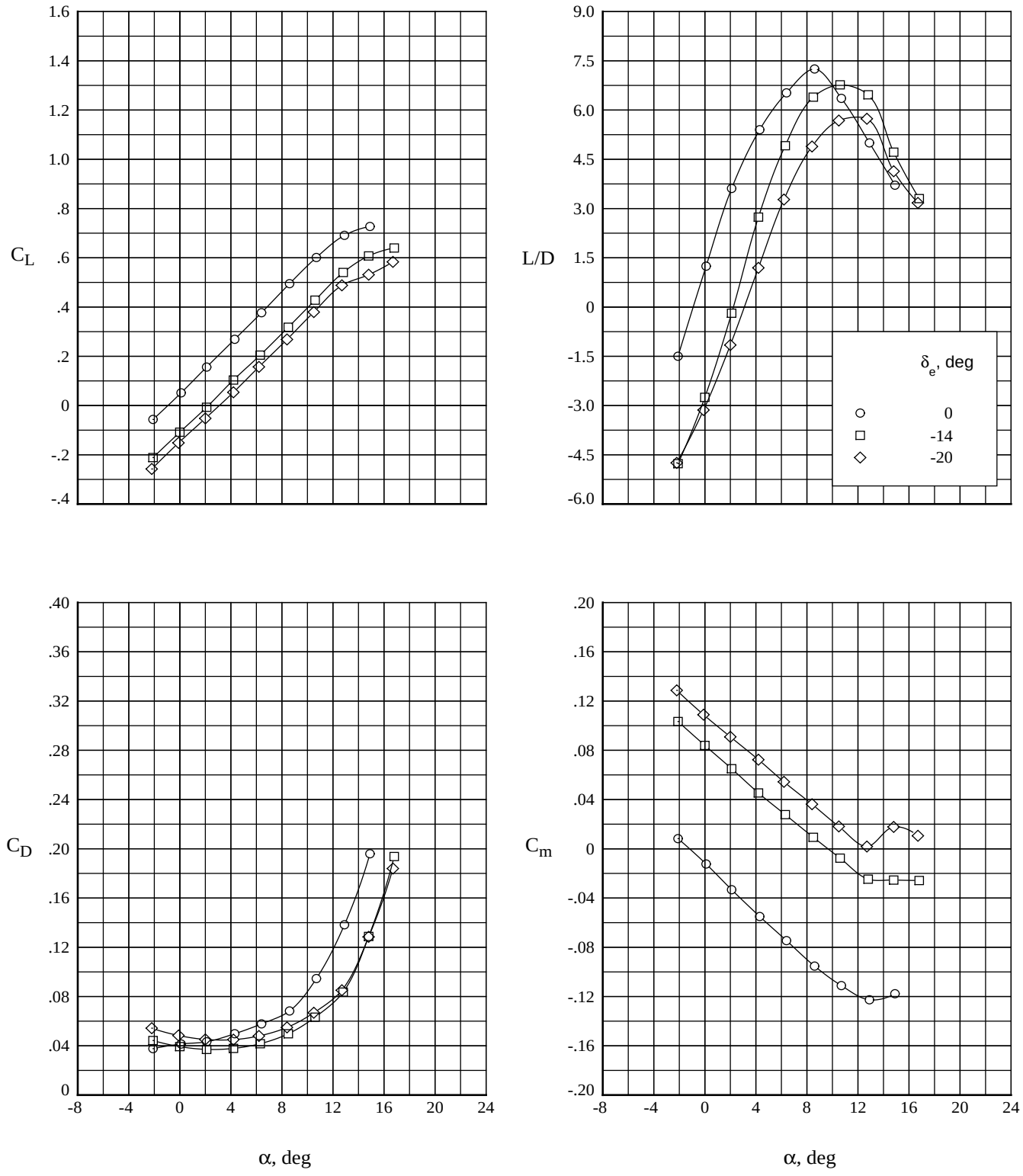

(b) Wingtip fins.

Figure 7. Continued.

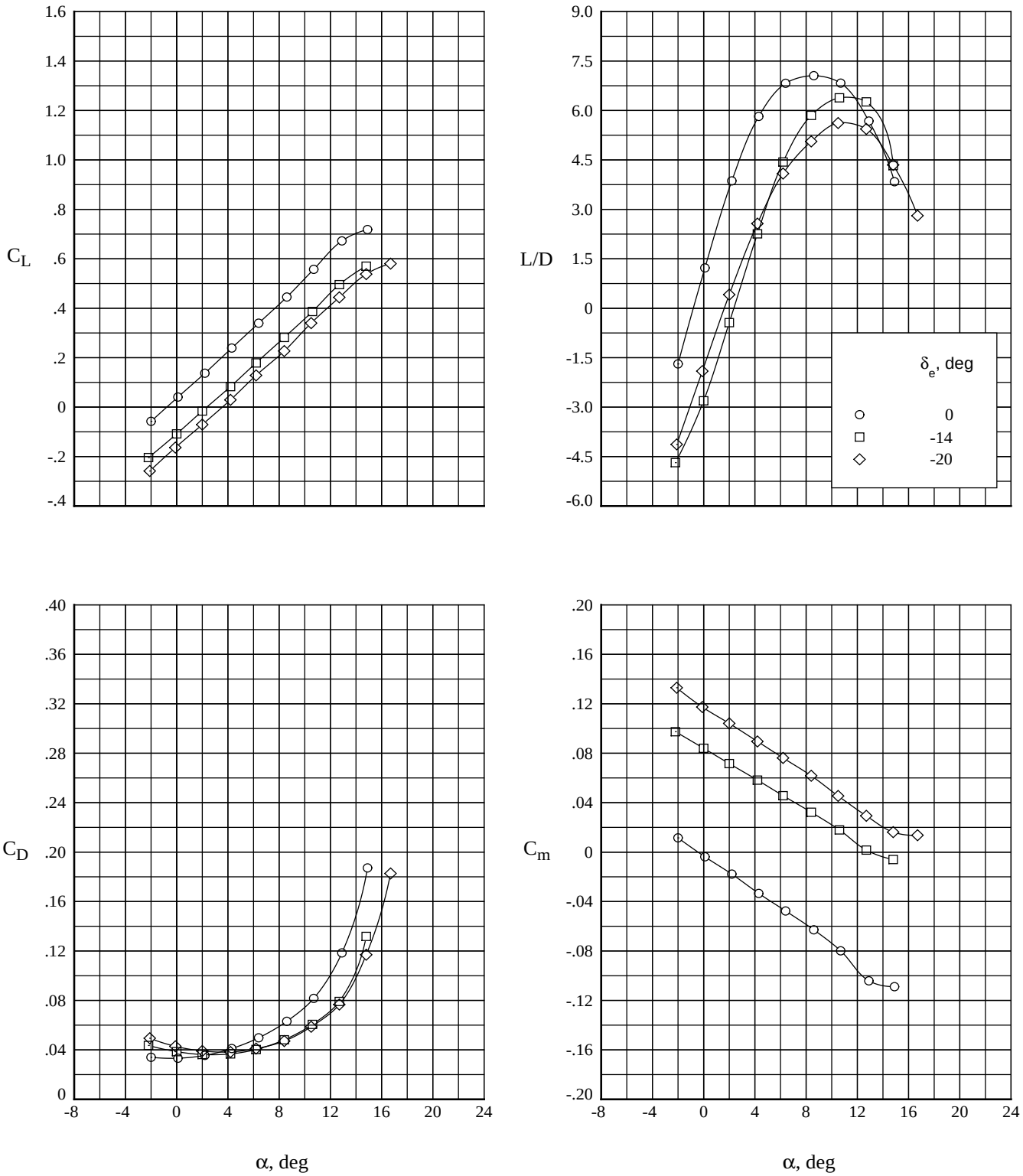

(c) Nose fin.

Figure 7. Concluded.

(a) $\alpha = 6.35°$.

(b) $\alpha = 10.64°$.

(c) $\alpha = 12.80°$.

(d) $\alpha = 14.83°$.

Figure 8. Oil flow on fins-off configuration at $M = 0.3$, showing upper surface of left-side wing with $\delta_e = -14°$.

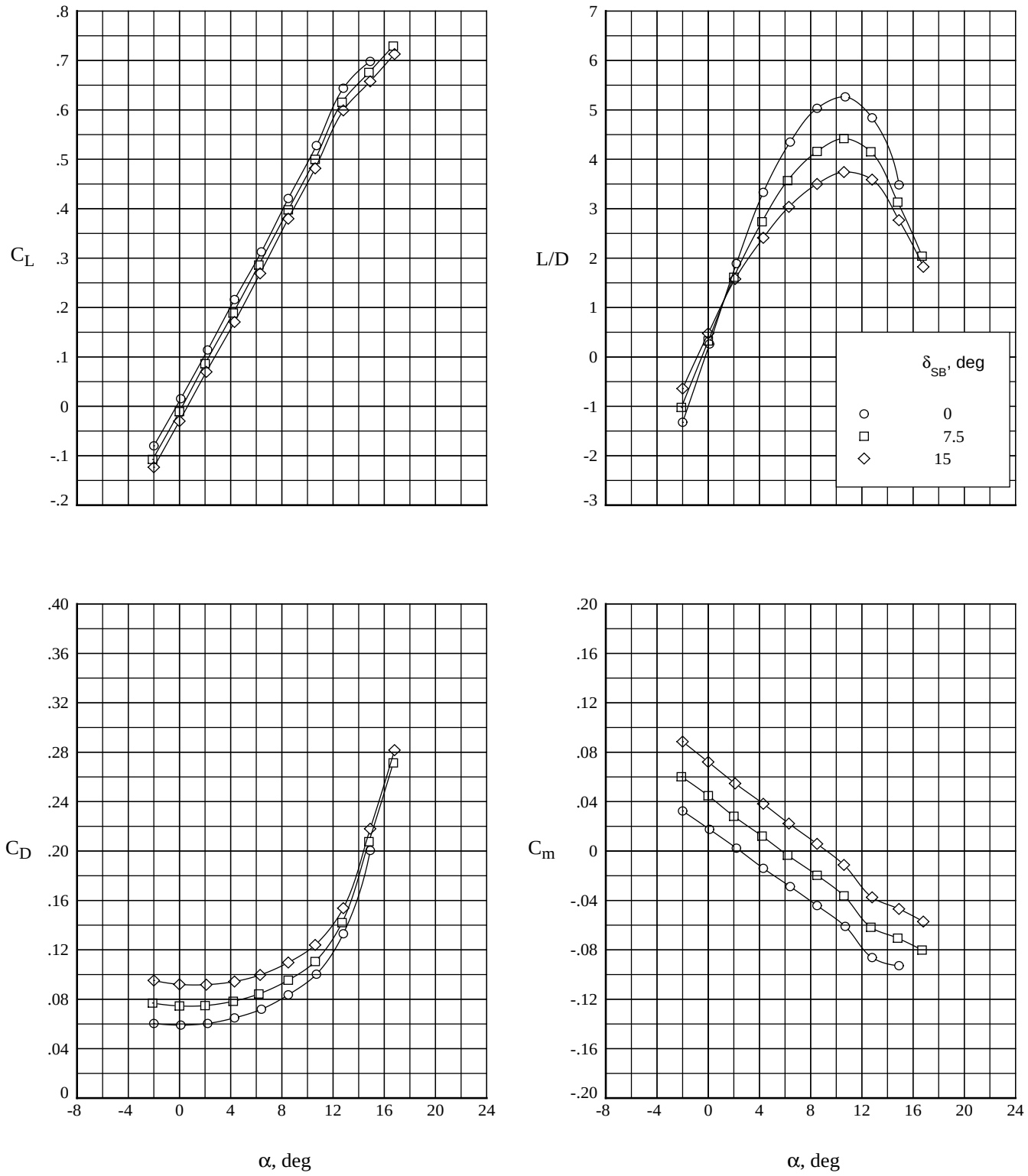

(a) Center fin.

Figure 9. Effect of speed-brake deflection on longitudinal characteristics of circular body model. $\delta_e = 0°$.

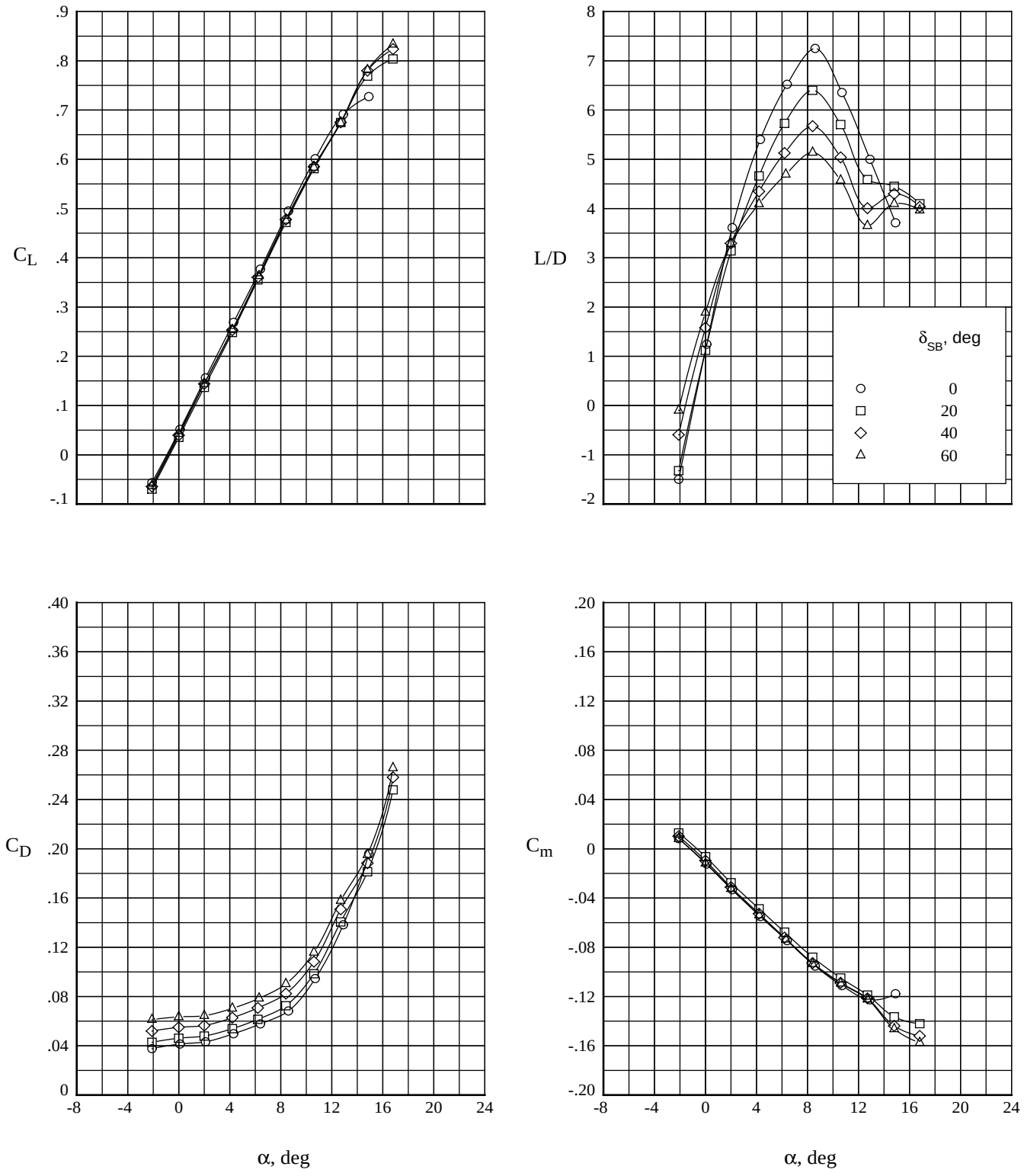

(b) Wingtip fins.

Figure 9. Continued.

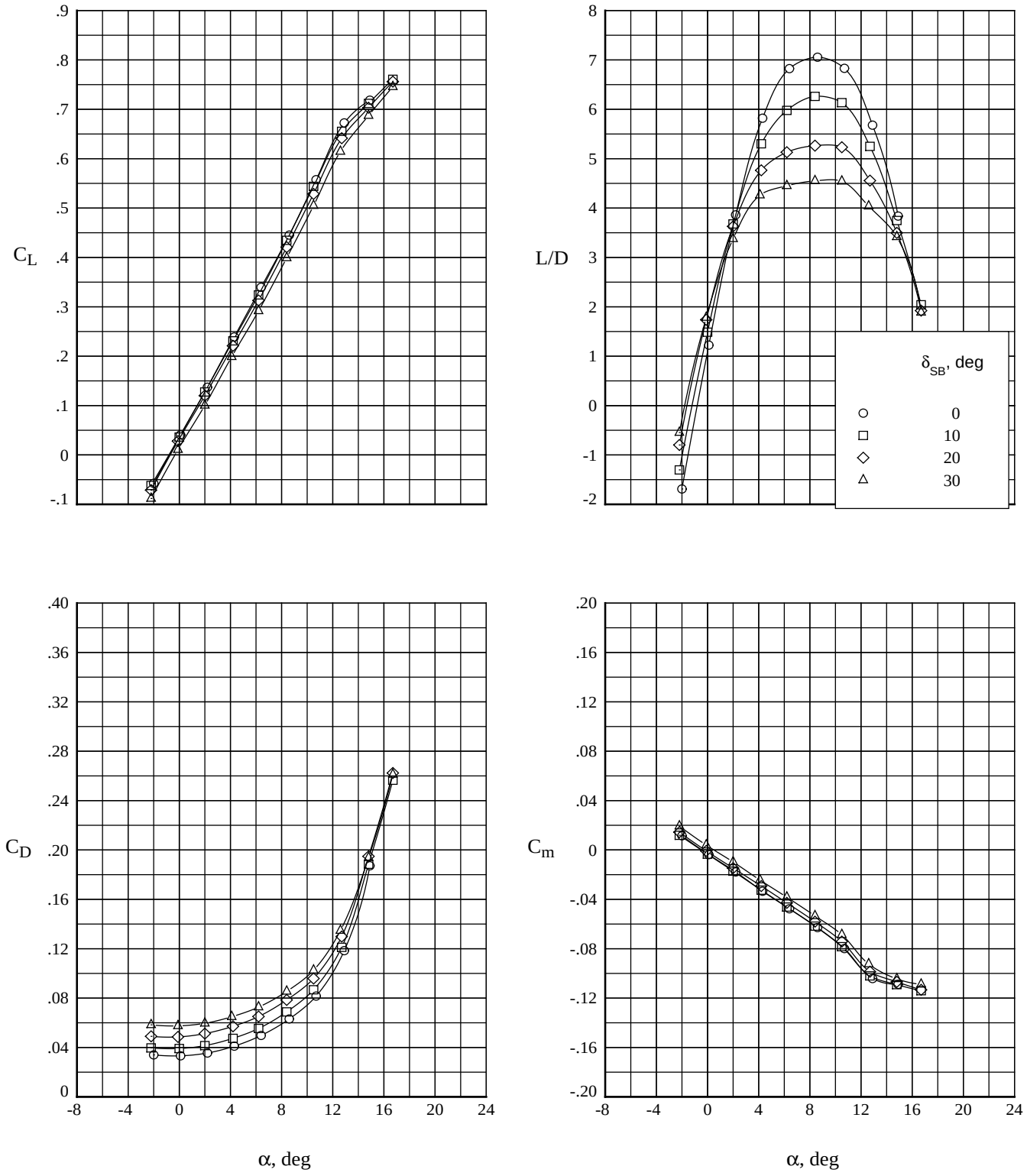

(c) Nose fin.

Figure 9. Concluded.

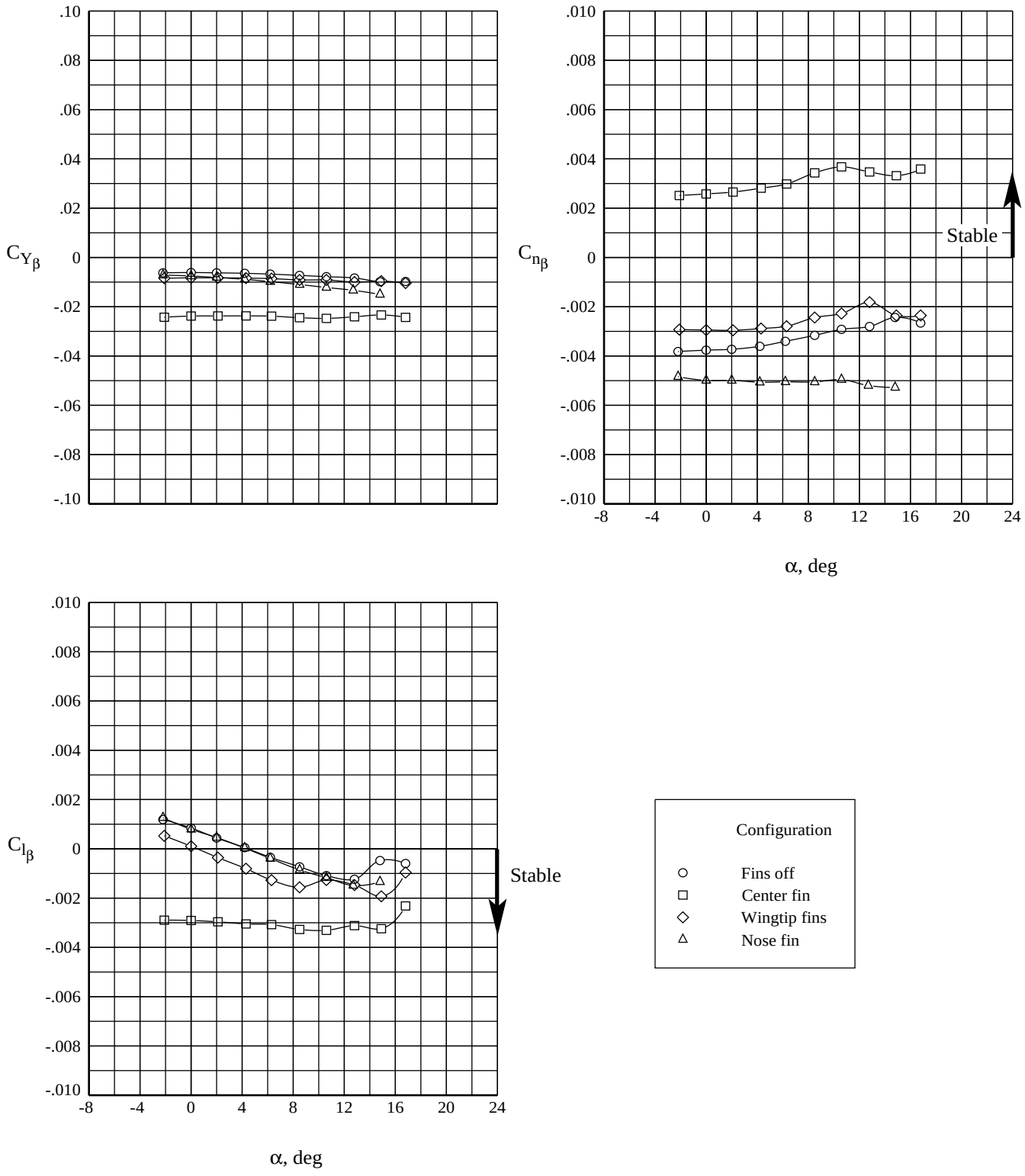

Figure 10. Lateral directional-stability characteristics of circular body model with various fin arrangements. $\delta_e = 0°$.

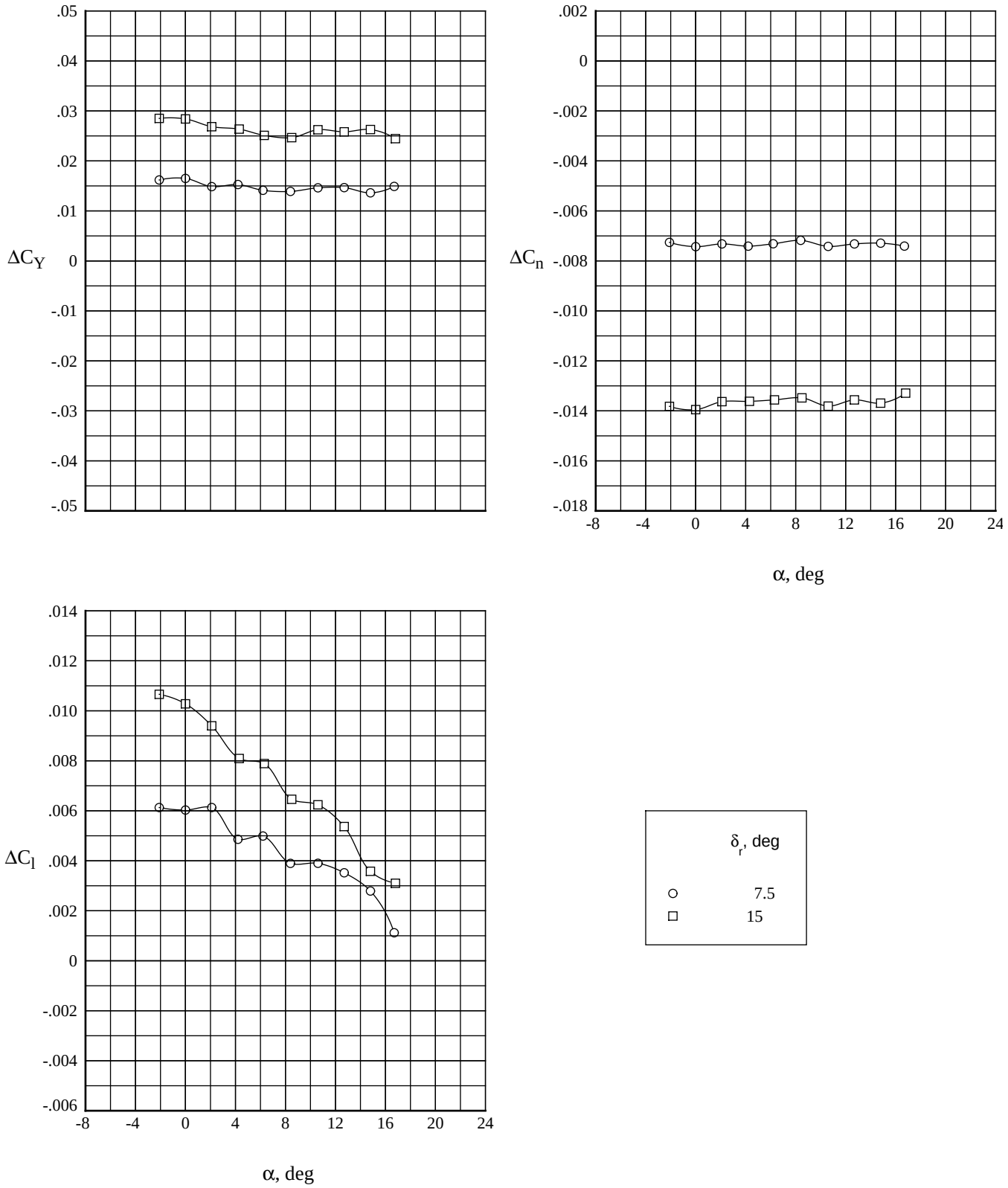

(a) Center fin.

Figure 11. Effect of rudder deflection as yaw control for circular body model. $\delta_e = -14°$.

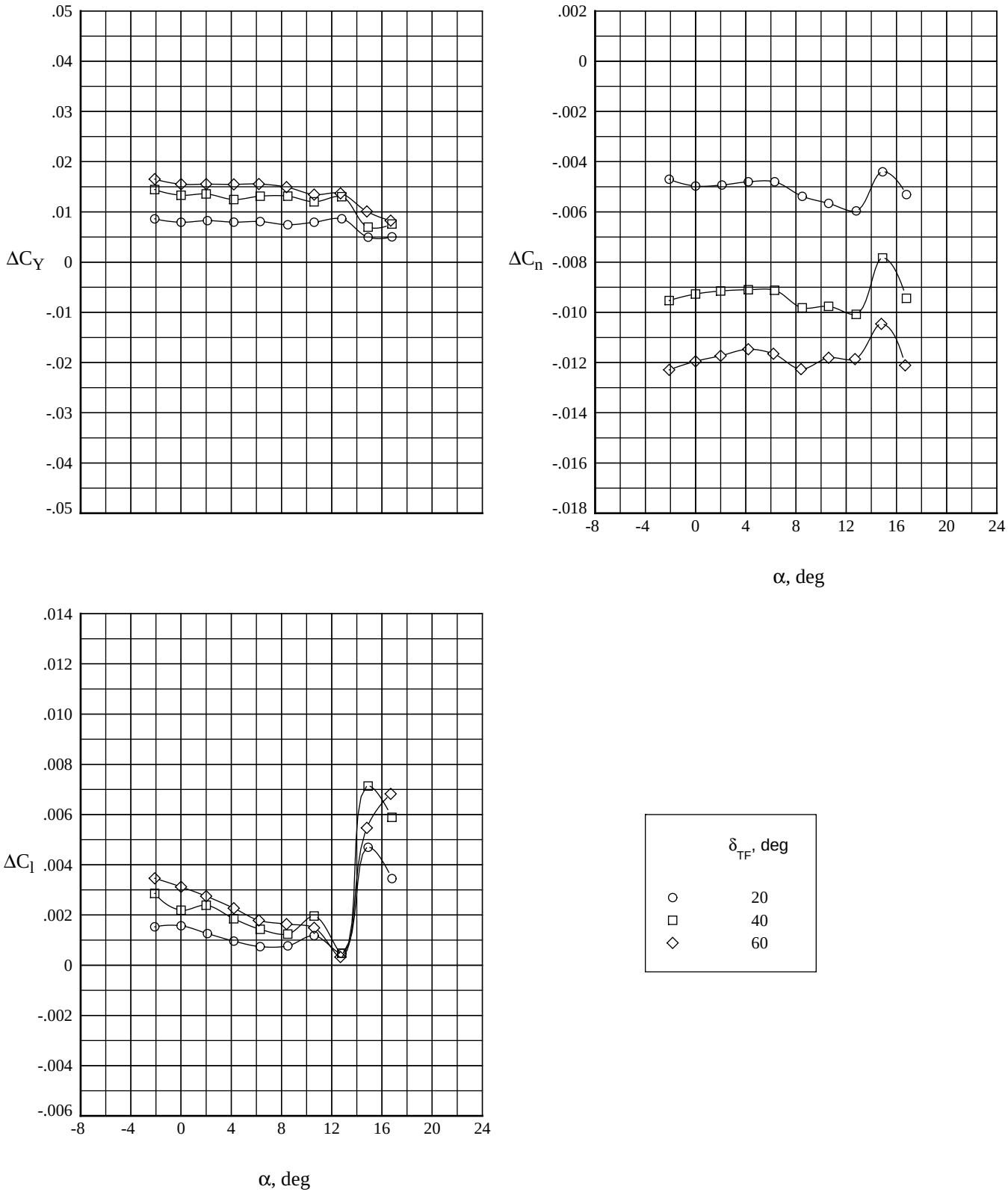

(b) Wingtip fins.

Figure 11. Continued.

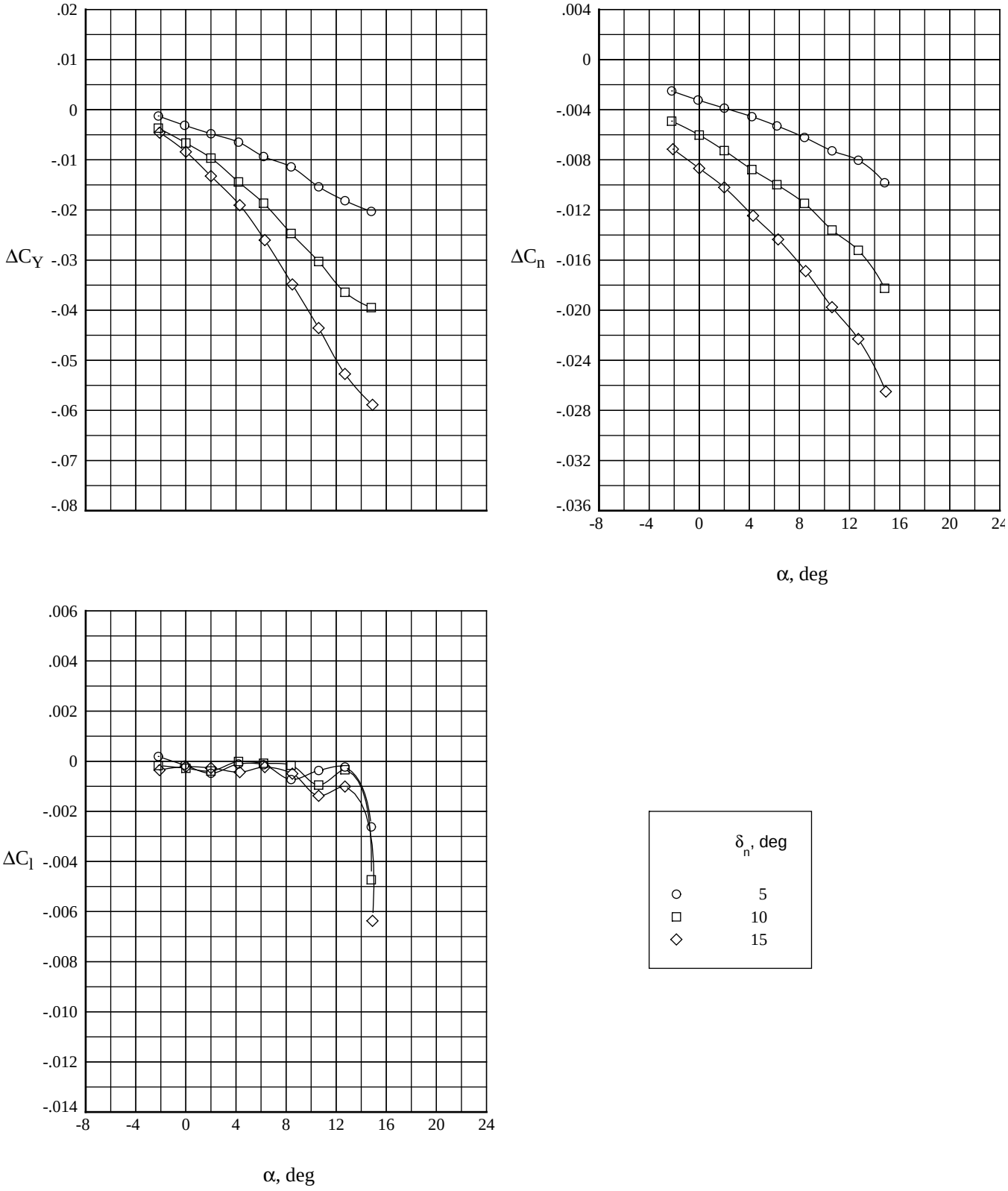

(c) Nose fin.

Figure 11. Concluded.

(a) $\delta_{TF} = 0°$.

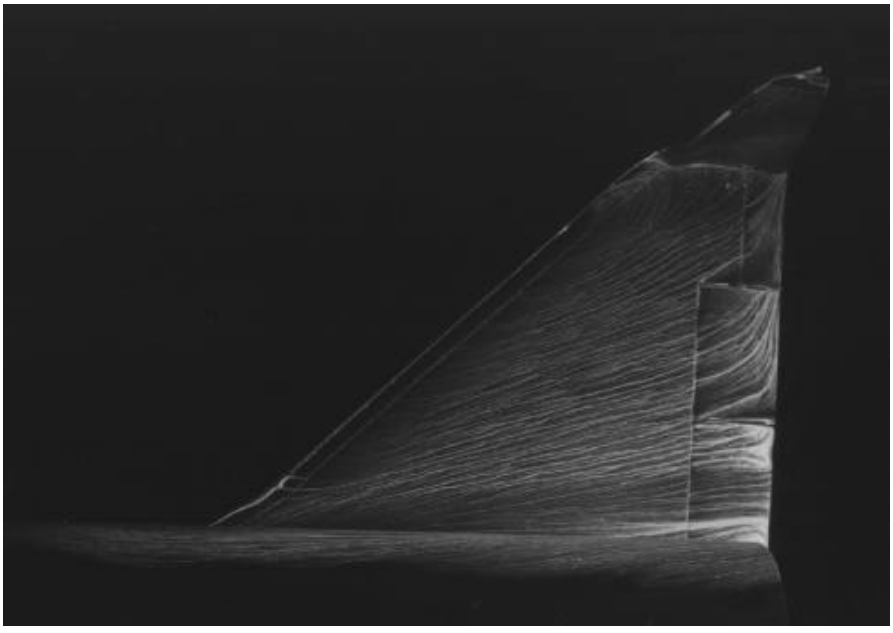

(b) $\delta_{TF} = 20°$.

Figure 12. Oil flow on tip-fin configuration at $M = 0.3$, showing right-wing upper surface, $\alpha = 12.86°$, $\delta_e = 0°$.

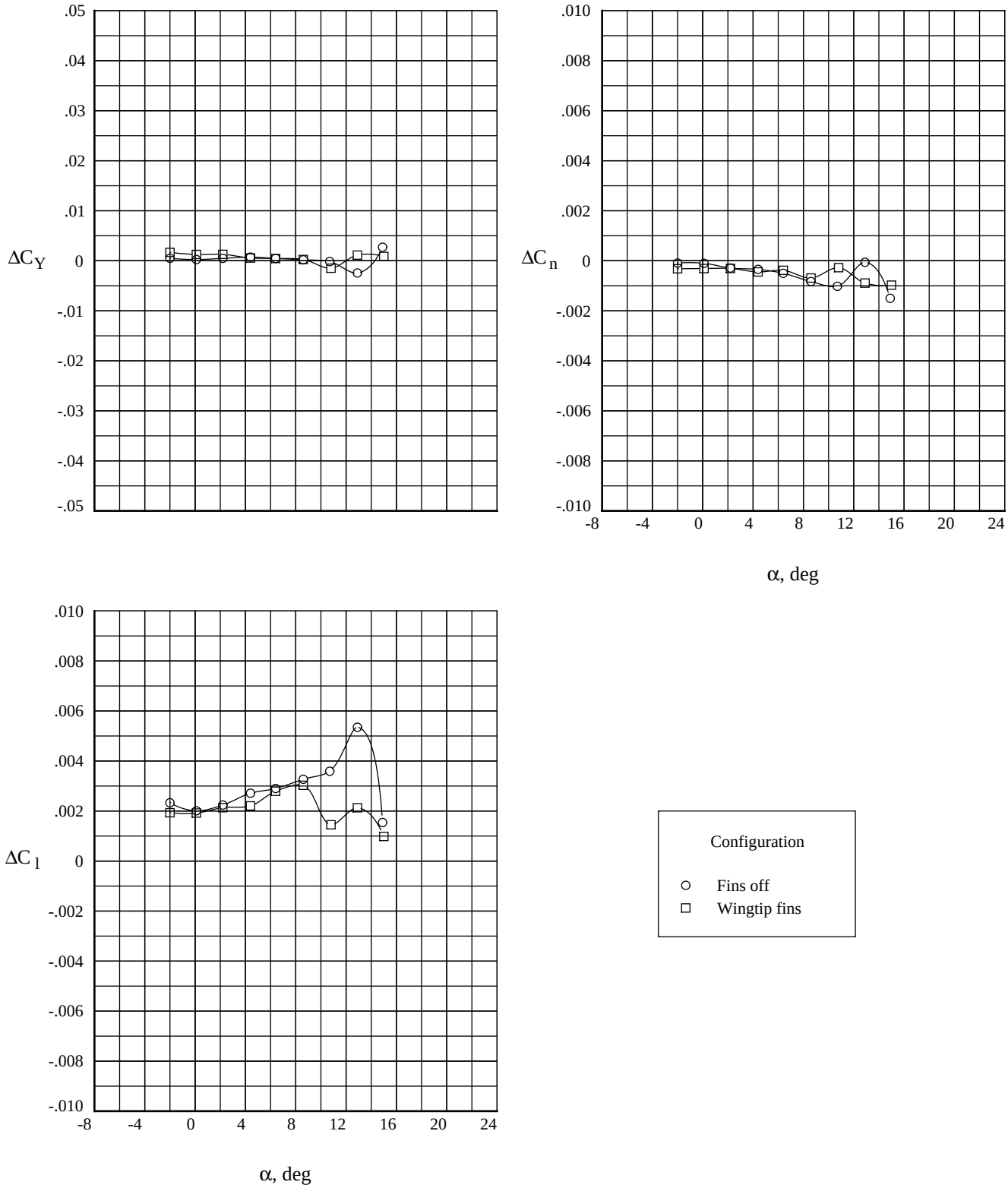

Figure 13. Effect of outboard ailerons as roll control for circular body model. δ_a = 5° and δ_e = 0°.

REPORT DOCUMENTATION PAGE

Form Approved
OMB No. 0704-0188

1. AGENCY USE ONLY *(Leave blank)*	2. REPORT DATE	3. REPORT TYPE AND DATES COVERED
	July 1996	Technical Memorandum

4. TITLE AND SUBTITLE
Subsonic Aerodynamic Characteristics of a Circular Body Earth-to-Orbit Vehicle

5. FUNDING NUMBERS
WU 242-20-08-01

6. AUTHOR(S)
Roger A. Lepsch, Jr., George M. Ware, and Ian O. MacConochie

7. PERFORMING ORGANIZATION NAME(S) AND ADDRESS(ES)
NASA Langley Research Center
Hampton, VA 23681-0001

8. PERFORMING ORGANIZATION REPORT NUMBER
L-17429

9. SPONSORING/MONITORING AGENCY NAME(S) AND ADDRESS(ES)
National Aeronautics and Space Administration
Washington, DC 20546-0001

10. SPONSORING/MONITORING AGENCY REPORT NUMBER
NASA TM-4726

11. SUPPLEMENTARY NOTES
Lepsch and Ware: Langley Research Center, Hampton, VA; MacConochie: Lockheed Engineering & Sciences Company, Hampton, VA.

12a. DISTRIBUTION/AVAILABILITY STATEMENT
Unclassified–Unlimited
Subject Categories 15 and 02
Availability: NASA CASI (301) 621-0390

12b. DISTRIBUTION CODE

13. ABSTRACT *(Maximum 200 words)*

A test of a generic reusable earth-to-orbit transport was conducted in the 7- by 10-Foot high-speed tunnel at the Langley Research Center at Mach number 0.3. The model had a body with a circular cross section and a thick clipped delta wing as the major lifting surface. For directional control, three different vertical fin arrangements were investigated: a conventional aft-mounted center vertical fin, wingtip fins, and a nose-mounted vertical fin. The configuration was longitudinally stable about the estimated center-of-gravity position of 0.72 body length and had sufficient pitch-control authority for stable trim over a wide range of angle of attack, regardless of fin arrangement. The maximum trimmed lift/drag ratio for the aft center-fin configuration was less than 5, whereas the other configurations had values of above 6. The aft center-fin configuration was directionally stable for all angles of attack tested. The wingtip and nose fins were not intended to produce directional stability but to be active controllers for artificial stabilization. Small rolling-moment values resulted from yaw control of the nose fin. Large adverse rolling-moment increments resulted from tip-fin controller deflection above 13° angle of attack. Flow visualization indicated that the adverse rolling-moment increments were probably caused by the influence of the deflected tip-fin controller on wing flow separation.

14. SUBJECT TERMS	15. NUMBER OF PAGES
Aerodynamics; Subsonic; Spacecraft; Booster	30
	16. PRICE CODE: A03

17. SECURITY CLASSIFICATION OF REPORT	18. SECURITY CLASSIFICATION OF THIS PAGE	19. SECURITY CLASSIFICATION OF ABSTRACT	20. LIMITATION OF ABSTRACT
Unclassified	Unclassified	Unclassified	